2020 16th IEEE International Conference on Automation Science and Engineering (CASE)
August 20-21, 2020, Online Zoom Meeting

Automated Single-microparticle Patterning System for Micro-analytics

Kaicheng Huang[1], Zhenxi Cui[1], Ihab Abu Ajamieh[2], Jiewen Lai[1], James K. Mills[2] and Henry K. Chu[1]*

Abstract— **Micropatterning has been applied in pharmaceutical research and drug discovery as an effective tool. Assays and tests can be easily performed by arranging microparticles in an array. However, the quality of the microparticle pattern influences the reliability of the results. In this study, an automatic single-microparticle patterning system was developed. This system enables precise patterning of single microparticles through dielectrophoresis, which can manipulate micro-objects (e.g., bead, protein, and cell). Orange fluorescent polystyrene beads ($40\mu m$) were suspended in 6-aminohexanoic acid solution. In contrast to the conventional microfluidic configuration, electrode-based microchip suspended above the substrate can selectively trap and pattern the microbeads. In particular, the microbeads laying on the substrate can be displaced to different positions relative to the patterning electrodes in the microchip. A vision-based approach was used to evaluate necessary information such as the gap distance and positions of the electrodes and microbeads in the image. Experiments were performed to examine the strategy used to construct high-quality single-bead patterns. With the proposed system, different single microbead patterns can be successfully constructed on a glass substrate. Results confirmed that this system offers an automatic method with high flexibility to construct different single microparticle patterns for various applications.**

I. INTRODUCTION

Microparticle patterning plays an important role, especially biological and pharmaceutical analytics. It arranges microparticles in an array via micromanipulation methods for high-throughput analysis. Various functions can be achieved through patterning with different microparticles. In the biomolecule scale, patterning receptor or antibody structure benefits to the protein chips [1] and immunoassay [2]. Cell-based patterning helps scientists focus on cell studies. Zhou et al. [3] combined high-content imaging (HCI) and on-chip microarray for single-cell analysis, because HCI is a useful tool for cellular heterogeneity and cell signal analysis. Sims et al. [4] applied polymerase chain reaction (PCR) in a single-cell patterning chip for mammalian cell analysis. Kim et al. [5] patterned mouse embryo fibroblast cells and analyzed lipid inhibition activity by using anti-obesity agents. Liu et al. [6] used a microfluidic chip with poly(ethylene glycol) microarray to hold cancer cells in an array for drug testing. Using a tap-assisted photolithographic-free microfluidic chip, Zhao et al. [7] studied tumor metastasis by arranging cells in a pattern.

LOC devices have been widely used for biological and chemical assays [8]. These devices, also known as micro total analysis systems, are essentially a mini laboratory embedded on a small chip [9] that can carry out one or more laboratory functions. Various methods are proposed as LOC devices for micropatterning. As one of the commonly used tools in the field, dielectrophoresis (DEP) is advantageous because the target object needs no pretreatment. Pretreatment introduces some chemicals that can damage biological particles (e.g., cells). Therefore, DEP is widely applied in biological particle patterning [2], [10]–[13]. In a common electrode-based microfluidic device that employs the DEP technique, the shape and appearance of the electrodes are first decided in accordance with the application. On the basis of the electrode design, a conductive electrode layer is printed on a glass slide with photolithography technology. Although the microfluidic devices can solve specific problems, each microchip is uniquely designed for its intended application. Pattern performance is determined by the electrode configuration and other parameters, such as microchannel size, which cannot be changed after fabrication.

Two methods, namely, light-induced DEP and optical-tweezers can aid researchers to arbitrarily create different microparticle patterns. Both methods rely on a robotic-aided light beam system to induce the translation of particles. By manipulating and controlling the beams, which focus on the substrate, the particles on the substrate can be transferred to different positions, thereby forming various patterns. Yang et al. [14] patterned and manipulated individual HepG2 cells and polystyrene (PS) beads with an organic photoconductive chip through light-induced optoelectronic DEP force. Yan et al. [15] applied a multilevel-based topology design with optical-tweezers to scale and rotate the desired cell pattern. Although these two techniques overcome the restriction of traditional DEP, some drawbacks still exist. In particular, both of these devices have a limited number of light beams, so only a small number of microparticles can be transferred simultaneously. Thus, a universal platform is needed to implement micropatterning.

A robot-aided electrode-based microchip is suggested to solve this problem. This microchip can selectively generate electric fields to trap and manipulate microparticles. As the microchip can be arbitrarily designed, the number in the electric field generation has no limitation. In our previous work, a four-by-four dot electrode array microchip was designed to generate ring-like electric fields for constructing cell cluster patterns via negative DEP (n-DEP) [16]. The microchip was placed in a linear platform so that a large-

[1]K. Huang, [1]Z. Cui, [1]J. Lai and [1]H. K. Chu are with the Department of Mechanical Engineering, The Hong Kong Polytechnic University, Hong Kong.(*Corresponding Author, email: henry.chu@polyu.edu.hk)

[2]J. K. Mills, [2]I. A. Ajamieh are with the Department of Mechanical and Industrial Engineering at the University of Toronto. Toronto, Ontario, Canada

A supplementary video can be found here: https://huangkc0907.github.io/portfolio/

scale cell cluster pattern can be printed on the same substrate and form a series of cell cluster characters [17]. The system was tested by printing cell patterns on various substrates to demonstrate its flexibility for different applications [18]. In the resent study, the system was further enhanced to construct high-quality single-microbead patterns with feedback control. Micro-PS beads with orange fluorescent color were used in the experiments. The beads randomly suspended in an aqueous environment on the substrate were selectively held and trapped by the electric fields generated from the electrodes, thereby forming a microbead pattern. To prevent more than one bead from being trapped by the same electrode during patterning, vision-based algorithms were developed to manipulate the target bead toward the desired position with respect to the electrode such that the redundant beads near the target bead can be repelled by the electric field. Path planning was incorporated for bead manipulation to avoid the target bead from being influenced by local electric field minima or other electrodes. A PID controller was applied to the system to guarantee that the target bead was following the desired path. A series of tests was performed to validate the effectiveness and robustness of the system.

II. SYSTEM SETUP

A. Design of the micropatterning system

The main component of the system is a multi-layer microchip that uses the DEP technique to create non-uniform electric fields through electrodes for microparticle manipulation and trapping. For a dielectric particle, a net DEP force, $\boldsymbol{F}_{DEP}$, acting on the particle, can be evaluated as follows:

$$\boldsymbol{F}_{DEP} = 2\pi r^3 \varepsilon_m \cdot Re[K(\omega)] \cdot \bigtriangledown E^2 \tag{1}$$

where r is the particle radius, ε_m is the permittivity of the suspending medium, $\bigtriangledown$ is the Del vector operator, E is the root mean square of the electric field, and $Re[K(\omega)]$ is the real part of the Clausius-Mossotti factor:

$$K(\omega) = \frac{\varepsilon_p^* - \varepsilon_m^*}{\varepsilon_p^* + 2\varepsilon_m^*} \tag{2}$$

where ε_p^* is the complex permittivity of the particle and ε_m^* is the complex permittivity of the suspension medium. An n-DEP force is required to drive the beads toward the substrate underneath the electrodes for the arrangement and patterning of the beads onto a substrate.

The microchip consists of 16 circle-surrounding electrode pairs that can generate 16 individual ring-like electric fields

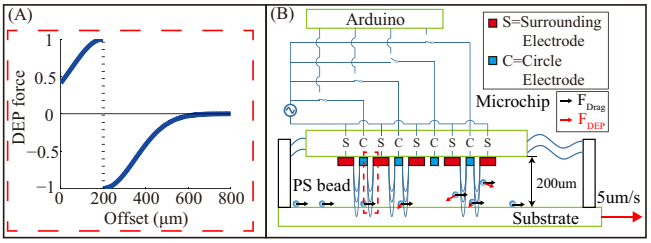

Fig. 1. (A). DEP force versus position (B). Sectional side illustration of micro bead trapped underneath the circle electrode

within a microenvironment to drive the beads toward underneath of the center of each circle electrode. The normalized n-DEP force acting on the bead with respect to its position as measured from the center of the circle electrode is shown in Fig. 1A. The DEP force on the bead located within the circle electrode with a radius of $200\mu m$ was directed to the center of the electrode, and the bead was trapped. Meanwhile, the bead located outside of the circle electrode was repelled. Thus, the electrodes were designed in a circle, to balance the force in the center of the area, and the bead was trapped in the center. An Arduino board was used to selectively energize the electrode pairs to trap the beads in different patterns, as shown in Fig. 1B. This figure also shows the force analysis of the beads underneath the circle electrode area or outside the area.

An adjustable microenvironment was created between the substrate and microchip through a sliding rail and a microscope (Leica DMi8) to enable relative movement between the microbeads and the circle electrodes in the microchip. This microscope is equipped with a motorized stage and a vertical stage to adjust the objective lens. The microchip was attached to the sliding rail through a 3D printed chip-holder, which can provide motion for the microchip along the optical axis of the microscope. The position of the chip-holder can be controlled using another Arduino board, as shown in Fig. 2A. The microbeads suspended on the substrate were displaced to the area underneath the circle electrodes through the motorized plane movement stage, and the electrodes were turned on to trap the microbeads. Different patterns can be constructed by selecting the moving beads and energizing the electrodes. A vision-based microchip positioning method was used to evaluate image sharpness using the microchip and substrate. This method was also used to measure and adjust the gap distance between the microchip and the substrate by sending a signal to the Arduino board and controlling the height of the microchip through the sliding rail. A gap distance of $200\mu m$ was applied in this study. A control interface was developed using the C++ program, which can display images from the microscope to facilitate coordinated movements among the linear stage, motorized platform, and vertical stage. The complete setup of the automatic bead patterning system is shown in Figs. 2C and 2D.

B. Material

PS beads with a diameter of $40\mu m$ and density of $1.05g/cm^3$ were suspended in 6-aminohexanoic acid (AHA) solution (Ruibio) to increase the buoyancy force acting on the beads and minimize the influence caused by the adhesion force from the substrate. The AHA solution was adjusted to 2.8M to increase the density ($\rho = 1.0798g/cm^3$) and PS beads were added to yield a concentration of 0.02% w/v.

Glass slides were used as the substrate for bead patterning. The glass substrate was treated with an Expanded Plasma Cleaner (Harrick Plasma, USA) for $10s$ prior to the experiments to induce polar functional groups, enhance surface hydrophobicity, and prevent the adherence of PS beads.

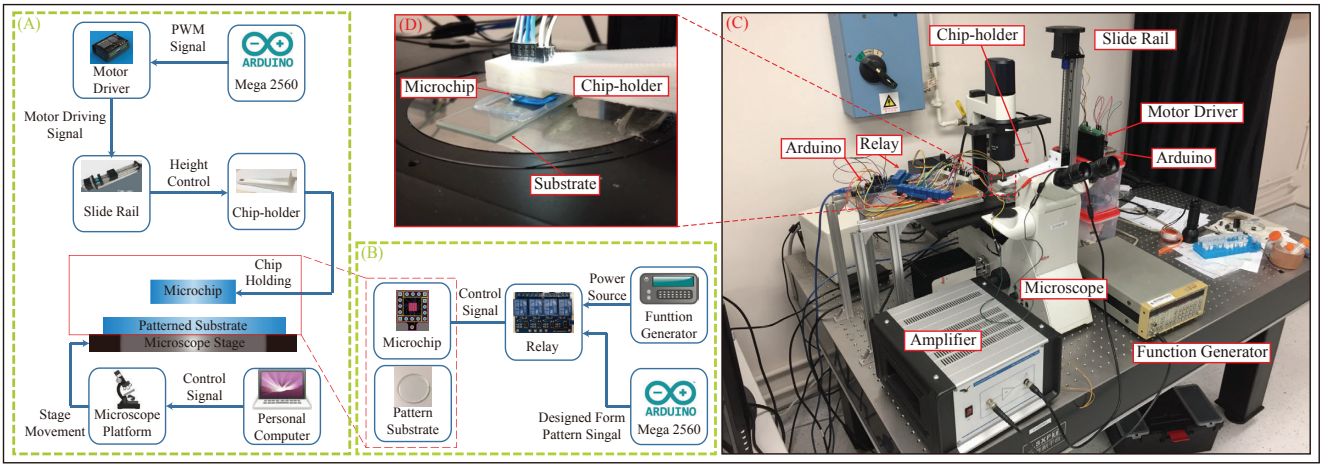

Fig. 2. (A and B). Diagram of the system setup (A). Components of the system mechanical setup (B). Components for generating selected output signals (C.D). Real image (C). Real image of the experimental setup (D). Zoomed view of the working area

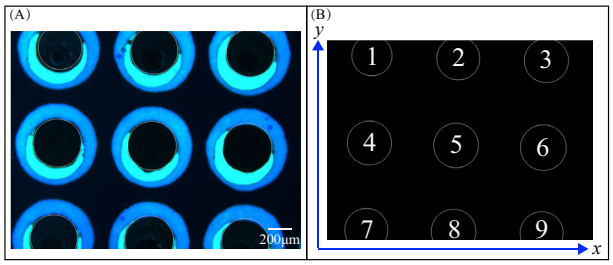

Fig. 3. Images of the microchip observed from the microscope (A). Using transmitted light (B). Using reflected light with electrodes labelled in white circles by the program

Thus, the surface property was changed from hydrophobic to hydrophilic.

C. Region detection and evaluation

Vision-based algorithms were developed to extract real-time information from the images and evaluate the positions between the electrodes and beads suspended in the solution. The computational time was reduced by converting the color images captured from the microscope into grayscale and then binary for image processing. Fine details were smoothened using a Gaussian filter, and image noises were removed by morphological operations. Some electrodes may not be completely captured because of the limited field of view of the microscope, as shown in Fig. 3A. The pixels in the image were grouped into multiple regions to separate the electrodes from the background. The largest region, which belonged to the surrounding electrode, was neglected, and the remaining regions were labeled as electrodes 1-9. Contours in the image were extracted using the algorithm proposed by Suzuki et al. [19] to evaluate the topological information of these regions. This algorithm can predict the entire geometry with only parts of the information provided, and the centers and radii of individual electrodes can be calculated, as shown by the white lines in Fig. 3B.

III. SINGLE BEAD TRAPPING

Fig. 1 illustrates the experimental procedure. The AHA solution with PS beads was dispensed on the substrate. The microchip was lowered to be immersed in the medium at $200\mu m$ above the substrate through the automatic microchip positioning function of the system. After obtaining the position information of the PS beads and electrodes with the detection function, a trapping strategy was used to obtain the trapping sequence for the PS beads. The PS beads were transferred to the bottom of the corresponding electrodes for trapping through the motorized platform with a speed of $5\mu m/s$. Depending on the pattern, the electrodes on the microchip were selectively powered on to trap the PS beads. The formed microbead pattern was finally transferred to a clean region of the substrate.

A. Trapping strategy

For precise single-bead patterning, individual electrodes were energized by the sequence (Fig. 3B) to trap the beads that were sequentially moved underneath of each electrode through the stage. The simulation in Fig. 4A shows the simulation of the electric field generated from the microchip, where high-strength field gradients occurred at the inner and outer boundaries of the electrodes. With this ring-like electric field, the PS beads were trapped in the center of the dot electrode. However, according to the simulation, the beads could also be trapped in the diamond-like zones (Fig. 4A), as the beads in this area may experience balanced DEP forces generated from the four surrounding electric fields.

Finding the top bead (in the image coordinate shown in Fig. 3B) rather than the bead nearest to the electrode, which is prepared to be activated, is the strategy used to select the bead for patterning. Thus, undesired beads were prevented from being trapped in the diamond-like zones. These areas were cleaned when the four surrounding electrodes were energized, because selecting the top bead for patterning guaranteed no redundant bead was present above the electrode prepared to be activated. For example, electrodes 1, 2, and 4 were already activated, and electrode 5 was prepared to be turned on. If a bead exists in the diamond-like area, this bead would be trapped after electrode 5 is powered on. Fig. 4B shows the possible outcome for not using the top-bead patterning strategy, which resulted in the bead being trapped in the diamond zone. As shown in Fig. 4C, a single bead

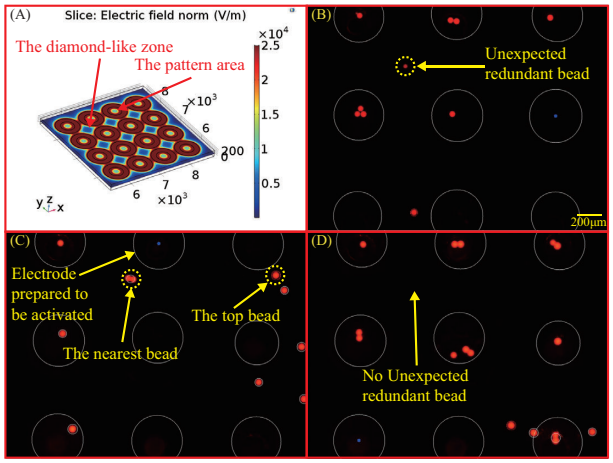

Fig. 4. (A). Simulation of the electric field from the microchip (B). Patterning result with "nearest-pattern" strategy (C). Diagram showing the "top-pattern" strategy (D). Patterning result with "top-pattern" strategy that can avoid unexpected beads

and a pair of beads were near the second electrode which was prepared to be activated. Although the beads in pairs were nearer to the electrode, the top one (labeled with a red circle) should be the target bead for patterning. Therefore, no bead was trapped in the diamond-like zone (Fig. 4D).

Fig. 5 shows a top-view illustration of the patterning procedure for the top-bead patterning strategy. First, all beads within the image were located and the top bead was chosen to be manipulated toward the first electrode for patterning (Fig. 5A). Through the motorized platform of the microscope system, the substrate and suspending beads were moved together for the top bead to be positioned within the boundary of the electrode (Fig. 5B). The electrode was energized to hold the bead via the DEP force. The procedure

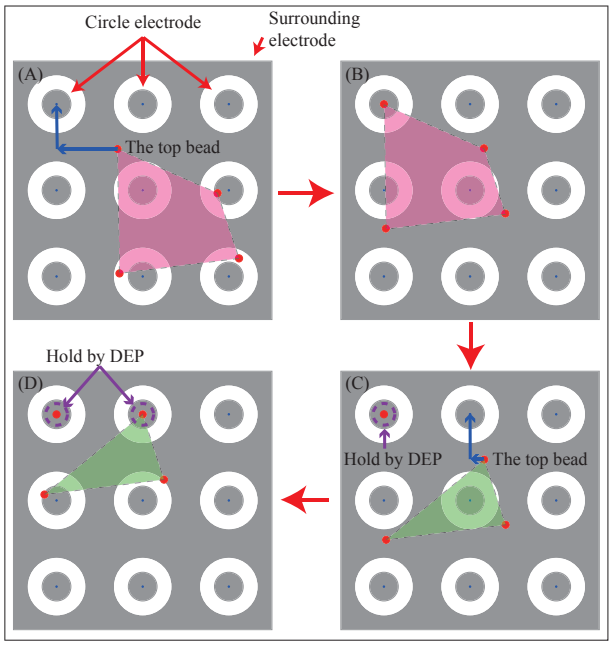

Fig. 5. Procedure of bead patterning from the top view (A). The top bead was moved to the first electrode through the microscope platform (B). The first electrode was energized (C). The top bead in the remaining beads was moved to the second electrode (D). The second electrode was energized

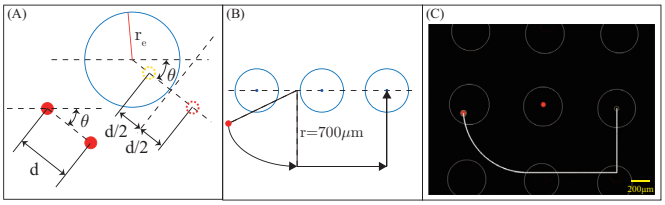

Fig. 6. (A). Diagram of bead separation (B). Diagram showing the details of the path (C). Path drawn on the image

was repeated (Figs. 5C and 5D) until all electrodes were utilized for patterning. The sequence of the electrode that should be activated follows the number shown in Fig. 3B.

The concentration of the PS beads in the solution is highly correlated with the number of beads present in the field. When the concentration is low, the number of beads may not be sufficient to provide beads for every electrode. For example, as shown in Fig. 5, no more beads were available after the fourth electrode was energized. In this scenario, the platform would continuously move in the upward direction (image) to search for more beads for patterning. This approach may take a long time to complete the patterning process, and increasing the concentration could help provide more beads at the initial state for patterning. However, this increase could also lead to a high possibility of beads that are close to one another. Limiting one bead to fall within the boundary of the electrode is difficult because the diameter of the electrode is relatively large. Multiple beads could be driven to the center of the electrode, as shown in the region of electrodes 2 and 4 (Fig. 4B).

B. Single bead patterning with path following

Only one bead is ideally allowed to be trapped by each electrode. As discussed, the nearby beads around the target bead could also be trapped by the same electrode. The electric field could be used for effective bead separation, allowing only one bead to be trapped.

Fig. 4A shows that the highest electric field occurred at the boundary of the electrode, and the strength of the electric field decreased as the distance to the boundary of the electrode increased. Thus, for an electrode with a radius of $200\mu m$, the direction and strength of the DEP force changed considerably from the inner and outer sides of the boundary. The normalized figure is shown in Fig. 1A. A search-and-evaluation method was employed to generate the path based on the relative position information between the top and nearest beads and find the optimal position for bead separation. The top bead was displaced underneath the center of the electrode when the distance of separation (d) was larger than $200\mu m$. The orientation of the nearest bead with respect to the top bead (θ) was evaluated when the distance of separation is less than $200\mu m$. The top bead was laid on the radius line, whose angle relative to the horizontal line was also θ, to maximize the distance for bead separation, The distance between the beads and electrode boundary was referred to as $d/2$ (yellow and red circles in Fig. 6A).

When the adjacent electrode from the same row was energized, the required path for the next electrode needed

to be planned properly. If the top bead needs to travel across the electric field generated by other electrodes, it could be forced to change the direction of movement or even stopped. The results show that the induced n-DEP force reached up to $700\mu m$ from the center of the circle electrode. A $700\mu m$ radius circular path, whose center lies on the same horizontal line with the bottom activated electrode, was set in advance to avoid the interference, moving the bead under (image coordination) the bottom area affected by the electric field, as shown in Fig. 6B. After the curved movement, the bead went laterally and vertically to the desired position, as shown in Fig. 6C.

A PID controller was used for path following to ensure the bead followed the desired path and precisely reached the desired position. The PID controller can be obtained as follows:

$$c(t) = K_p e(t) + K_i \int_0^t e(\tau)\, d\tau + K_d \frac{de(t)}{dt} \tag{3}$$

where $c(t)$ is the control input (in the relative position [μm]) for the microscope stage, and $e(t) = x^d(t) - x(t)$ is the position error between the desired $x^d(t)$ and actual $x(t)$ tracked bead positions. A region of interest was drawn at the current bead position and used to search for the new position to obtain the actual position of the bead in the next step, $x(t+1)$. Its position was updated at each iteration and restricted to 5 pixels width when finding the bead.

As the patterning procedure and bead movement were executed simultaneously, several beads were already being trapped when the target bead for patterning in the next step was tracked. The relationship between the DEP force and relative position between the electrode and PS bead is shown in Fig. 1A. The relationship is a segmented function, that is, the direction of the force differ among each side of the border $x_o = 200\mu m$, which is similar to the optical tweezers [20]. Therefore, an analogous controller needs to be designed to fulfill the requirement of the patterned beads, that is, they must not be brought through the attracted area. The input for the system is calculated as follows:

$$u(t_o) \begin{cases} c(t_o), & |c| < x_o \quad (4a) \\ x_o, & c \geq x_o \quad (4b) \\ -x_o, & -c \leq -x_o \quad (4c) \end{cases}$$

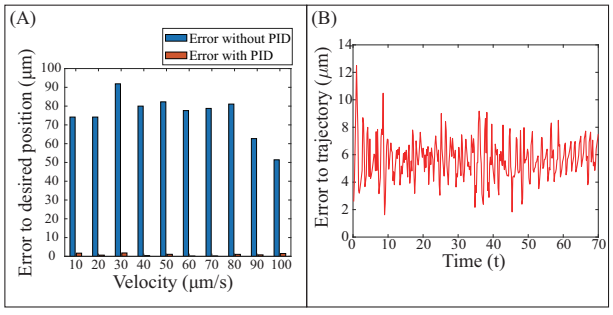

Fig. 7. (A). Error of the desired position with different velocities (B). Tracking performance on a curved path

IV. RESULTS AND DISCUSSION

A series of experiments was conducted to examine the performance of the proposed system for single-bead patterning. First, the use of PID for bead positioning was examined, and the error between using and not using PID control was compared with the platform moving at different velocities. Subsequently, the effectiveness of bead separation was evaluated. The beads separated at various distances were tested to determine the relationship between the success rate and separation distance. Finally, the automatic micropatterning system combined with the proposed patterning strategy could successfully construct a PS bead pattern on a glass substrate to demonstrate its feasibility and performance.

A. Single bead trapping

The parameters used in the PID controller are as follows: control gain $K_p = 0.6$, $K_i = 0$, and $K_d = 0.001$; and time constant $T_f = 0.2s$. Fig. 7A shows the result of using and not using the PID controller in PS bead translation. Without the PID controller, a position error occurred between the actual PS bead position and the desired bead position after manipulation of at least $50\mu m$, regardless of how fast the velocity of the platform was set. The large error was due to the relative displacement between the bead and substrate during movement. As shown in Fig. 1B, the movements of the PS beads were primarily induced by the drag force of the solution. However, the flow of the solution was complex and unpredictable, that the movements of the beads were also slightly unexpected. With feedback control, this error could be reduced to almost zero through PID tracking. Fig. 7B shows the performance of the controller, that is, moving a PS bead and following a curved path with the platform moving at $5\mu m/s$. The bead could efficiently follow the desired path with an average error of $5\mu m$ throughout tracking.

The performance of the bead separation with PID control is shown in Fig. 8. The distance between the two beads (Fig. 8A) was much smaller than the radius of the electrode. After reaching the desired position, these two beads were automatically positioned at two different sides of the boundary (Fig. 8B). They were successfully separated after the electrode was turned on, leaving one bead in the patterning area (Fig. 8C).

The initial distance between the adjacent beads strongly influences the success rate of bead separation. For the beads that were already adhered together, the applied electric field did not affect separation because they were polarized together (Fig. 9). For the beads that were sufficiently close, the interference from the beads altered the electric field distribution near the boundary of the electrode, causing a problem in finding the crossover point (sign change in the DEP force) for bead separation. The success rate of the separation versus different initial distances is shown in Fig. 10. A high success rate can be guaranteed if the initial distance between the beads exceeds $40\mu m$. This condition can be satisfied using a low-concentration PS bead solution.

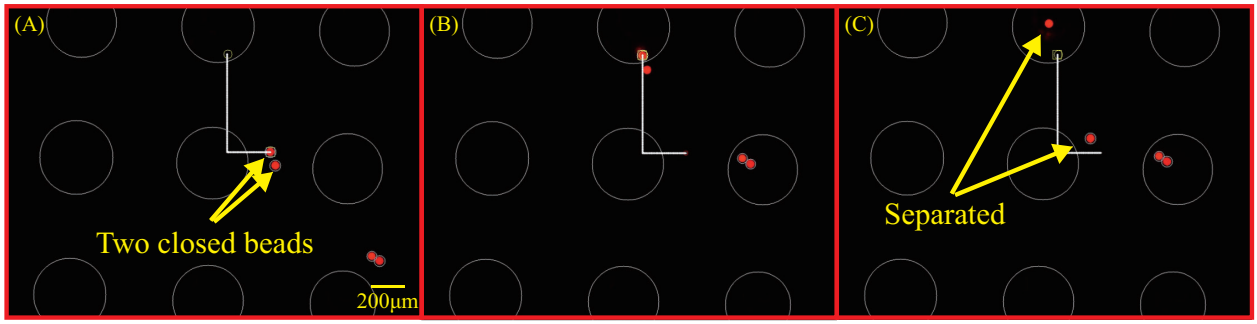

Fig. 8. Bead separation performance on two nearby beads (A). Calculate the optimal position for separating the two beads (B). Move the beads to the desired position (C). Turn on the electric field to attract one and repel the other

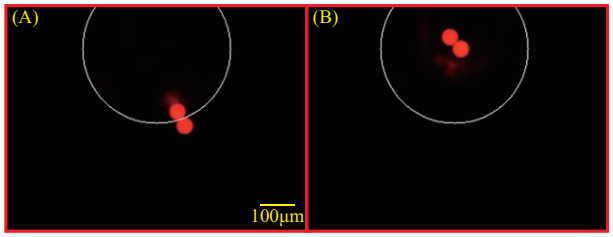

Fig. 9. Two adhered beads undergo bead separation (B). Both beads were trapped when the field was on

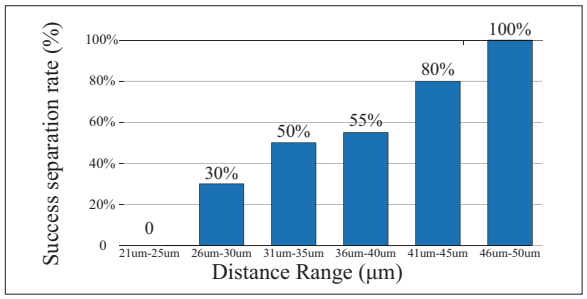

Fig. 10. Success rate of bead separation at different bead distances

B. Verification of automatic patterning program

The performance of the micropatterning system was also examined. The PS beads in the AHA solution were patterned on a glass substrate. In each step, the top bead was identified and the required path was generated, as illustrated by the white line in Fig. 11A. The bead was successfully manipulated to follow the path by using the PID controller. The corresponding electrode was turned on to hold the bead (Fig. 11B). Subsequently, the regions of the energized electrode were blocked in programming, indicating that the PS beads inside the electrode were no longer available for patterning even though they were in the upper position relative to the other beads (Fig. 11C). The bead separation method was also integrated into the system to achieve single bead patterning (Fig. 11D). When no more beads were available for patterning, the platform was moved upward to find new beads (Fig. 11E). The trapping force was sufficient in holding the patterned beads during searching and patterning. Following the procedure, nine PS beads were successfully trapped by the electrodes as a micro pattern, and this strategy prevented any beads from being trapped in the diamond-like areas. The final pattern is shown in Fig. 11F. The micropatterning system was also examined to demonstrate its effectiveness to create different patterns, including characters 'X' and 'T', and diamond shape (Fig. 12).

V. CONCLUSION

The scarcity of cell samples and high cost of drugs have lead to strong demand for accurate single-cell patterning. In this study, an automatic vision-based single micropatterning system was developed. This system can achieve high-accuracy single-microparticle patterning for micro analytics and consists of a height-adjustable microchip to facilitate easy detachment of the substrate after patterning. PS beads were chosen to test the accessibility of the system. Image processing techniques were used to extract the information for automatic bead selection and position evaluation. A separation method was used in the system to avoid multiple beads from being patterned by one electrode. In this method, the target beads were trapped and any nearby beads were repelled. A patterning strategy that locates the top bead was proposed and a collision-free path was generated for bead manipulation. A PID controller was adopted to guide the bead to follow the desired path. The experiments confirmed that the system can successfully pattern PS beads on a substrate with different designed forms by turning on the corresponding electrodes. The electrode-based microchip offers a cost-effective way to breakthrough the parallel-manipulated number limitation of robotic-aided multiple-point trapping methods, such as optical-tweezers and light-induced DEP. This microchip can also be easily adjusted to change the configurations (e.g., resolution) in accordance with the application. Compared with conventional LOC devices, separating the microchip with electrodes from the LOC device increases the flexibility of the system, thereby enabling precise control and selective trapping for single-particle patterning. This system provides an inexpensive, flexible, and effective method that uses n-DEP to create single microparticle patterns for biological particle assays and characterization.

REFERENCES

[1] M. R. Dusseiller, D. Schlaepfer, M. Koch, R. Kroschewski, and M. Textor, "An inverted microcontact printing method on topographically structured polystyrene chips for arrayed micro-3-d culturing of single cells," *Biomaterials*, vol. 26, no. 29, pp. 5917–5925, 2005.

[2] M. Yamamoto, T. Yasukawa, M. Suzuki, S. Kosuge, H. Shiku, T. Matsue, and F. Mizutani, "Patterning with particles using three-dimensional interdigitated array electrodes with negative dielectrophoresis and its application to simple immunosensing," *Electrochimica acta*, vol. 82, pp. 35–42, 2012.

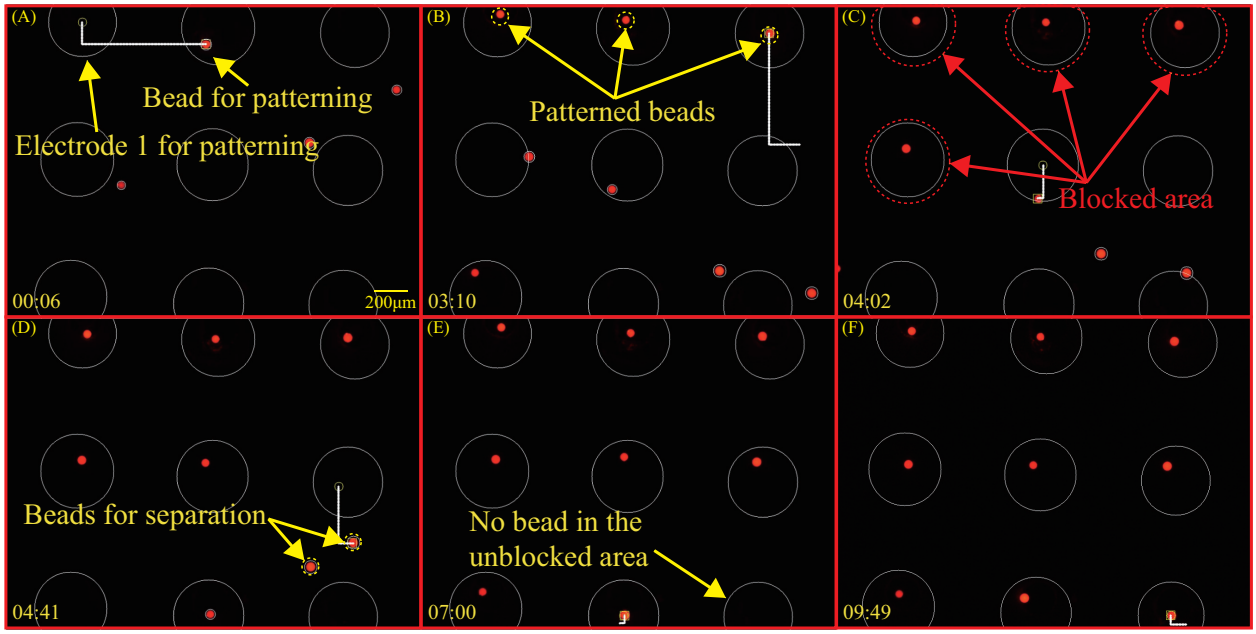

Fig. 11. Automatic patterning procedure of nine PS beads. Nine single $40\mu m$ beads can be patterned sequentially underneath the desired electrodes (white circles)

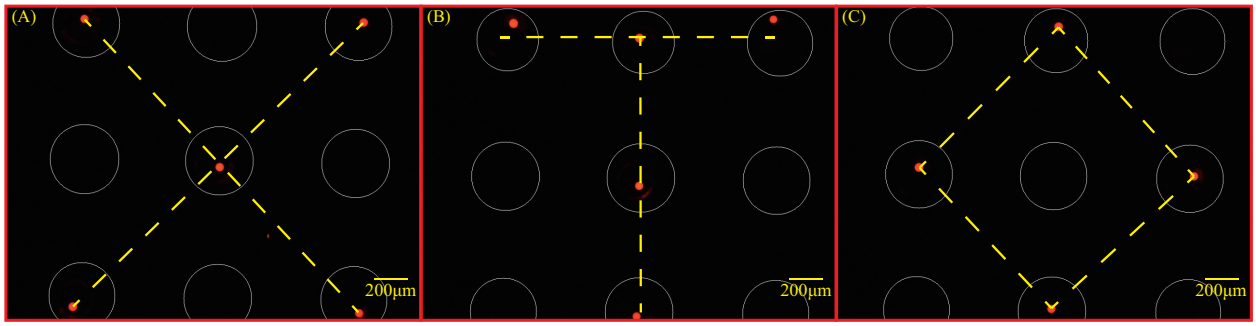

Fig. 12. Character pattern with PS beads (A). Character 'X' (B). Character 'T' (C). Diamond shape

[3] J. Zhou, Y. Wu, S.-K. Lee, and R. Fan, "High-content single-cell analysis on-chip using a laser microarray scanner," *Lab on a Chip*, vol. 12, no. 23, pp. 5025–5033, 2012.

[4] C. E. Sims and N. L. Allbritton, "Analysis of single mammalian cells on-chip," *Lab on a Chip*, vol. 7, no. 4, pp. 423–440, 2007.

[5] G. Y. Kim, S.-J. Yeom, S.-C. Jang, C.-S. Lee, C. Roh, and H.-H. Jeong, "Simple analysis of lipid inhibition activity on an adipocyte micro-cell pattern chip," *Biomolecules*, vol. 8, no. 2, p. 37, 2018.

[6] Z.-B. Liu, Y. Zhang, J.-J. Yu, A. F.-T. Mak, Y. Li, and M. Yang, "A microfluidic chip with poly (ethylene glycol) hydrogel microarray on nanoporous alumina membrane for cell patterning and drug testing," *Sensors and Actuators B: Chemical*, vol. 143, no. 2, pp. 776–783, 2010.

[7] L. Zhao, T. Guo, L. Wang, Y. Liu, G. Chen, H. Zhou, and M. Zhang, "Tape-assisted photolithographic-free microfluidic chip cell patterning for tumor metastasis study," *Analytical chemistry*, vol. 90, no. 1, pp. 777–784, 2018.

[8] S. Haeberle and R. Zengerle, "Microfluidic platforms for lab-on-a-chip applications," *Lab on a Chip*, vol. 7, no. 9, pp. 1094–1110, 2007.

[9] Y. Lim, A. Kouzani, and W. Duan, "Lab-on-a-chip: a component view," *Microsystem Technologies*, vol. 16, no. 12, pp. 1995–2015, 2010.

[10] K. Ino, H. Shiku, F. Ozawa, T. Yasukawa, and T. Matsue, "Manipulation of microparticles for construction of array patterns by negative dielectrophoresis using multilayered array and grid electrodes," *Biotechnology and bioengineering*, vol. 104, no. 4, pp. 709–718, 2009.

[11] A. Rosenthal and J. Voldman, "Dielectrophoretic traps for single-particle patterning," *Biophysical journal*, vol. 88, no. 3, pp. 2193–2205, 2005.

[12] S. Menad, L. Franqueville, N. Haddour, F. Buret, and M. Frénéa-Robin, "ndep-driven cell patterning and bottom-up construction of cell aggregates using a new bioelectronic chip," *Acta biomaterialia*, vol. 17, pp. 107–114, 2015.

[13] T. Horii, M. Yamamoto, T. Yasukawa, and F. Mizutani, "Rapid formation of cell-particle complexes via dielectrophoretic manipulation for the detection of surface antigens," *Biosensors and Bioelectronics*, vol. 61, pp. 215–221, 2014.

[14] S.-M. Yang, S.-Y. Tseng, H.-P. Chen, L. Hsu, and C.-H. Liu, "Cell patterning via diffraction-induced optoelectronic dielectrophoresis force on an organic photoconductive chip," *Lab on a Chip*, vol. 13, no. 19, pp. 3893–3902, 2013.

[15] X. Yan and D. Sun, "Multilevel-based topology design and cell patterning with robotically controlled optical tweezers," *IEEE Transactions on Control Systems Technology*, vol. 23, no. 1, pp. 176–185, 2014.

[16] K. Huang, H. K. Chu, B. Lu, and L. Cheng, "Characterization of a microchip device for cell patterning via negative dielectrophoresis," in *2018 IEEE International Conference on Robotics and Biomimetics (ROBIO)*. IEEE, 2018, pp. 1521–1526.

[17] K. Huang, H. K. Chu, B. Lu, J. Lai, and L. Cheng, "Automated cell patterning system with a microchip using dielectrophoresis," in *2019 International Conference on Robotics and Automation (ICRA)*. IEEE, 2019, pp. 634–639.

[18] K. Huang, B. Lu, J. Lai, and H. K. Chu, "Microchip system for patterning cells on different substrates via negative dielectrophoresis," *IEEE Transactions on Biomedical Circuits and Systems*, 2019.

[19] S. Suzuki *et al.*, "Topological structural analysis of digitized binary images by border following," *Computer vision, graphics, and image processing*, vol. 30, no. 1, pp. 32–46, 1985.

[20] S. Hu and D. Sun, "Automatic transportation of biological cells with a robot-tweezer manipulation system," *The International Journal of Robotics Research*, vol. 30, no. 14, pp. 1681–1694, 2011.